Chapter 1

Mechanical Behavior of Natural Hydraulic Lime Mortars

Lucía Garijo, XiaoXin Zhang, Gonzalo Ruiz,
José J. Ortega and Rena C. Yu

Additional information is available at the end of the chapter

http://dx.doi.org/10.5772/intechopen.80852

Abstract

Natural hydraulic lime (NHL) mortars are widely used for restoration works due to their good compatibility with the substrate material in terms of physical, chemical, and mechanical properties. Regarding their mechanical characterization, there is still a need for further understanding of their fracture behavior and the influence of their dosage methodology on the mechanical properties. Thus, this chapter focuses on the mechanical characterization of NHL mortars, such as flexural, compressive, and splitting tensile strengths, elastic modulus, and fracture energy. Moreover, the influence of the composition and production process on such properties was studied as well. Furthermore, the loading rate effect on the fracture behavior was also presented. The results show that NHL mortars have shape and size effect on the compressive strength. In addition, NHL mortar is rate sensitive, mainly due to the viscous effects caused by the presence of free water in the porous structure.

Keywords: mechanical characterization, dosage, empirical equations, size effect, loading rate effect

1. Introduction

Natural hydraulic lime (NHL) is a binding material formed by burning of argillaceous or siliceous limestones with reduction to powder by slaking with or without grinding [1]. From a mineralogical point of view, it is mainly composed of portlandite ($Ca(OH)_2$), dicalcium silicates (C_2S), gehlenite (C_2AS), and small amounts of tricalcium silicates (C_3S). Tricalcium aluminate (C_3A) and tetracalcium aluminoferrite (C_4AF) can be present as well [2]. Moreover,

calcite ($CaCO_3$) can also appear in NHL as a result of a slight carbonation (reaction with carbon dioxide from the air) of portlandite during storage [3]. When mixed appropriately with water and aggregates, NHL produces mortars which are able to harden and gain strength with time [1]. As a hydraulic material, NHL mortars have the property of setting and hardening under water and reacting with carbon dioxide from the air (carbonation) [1, 4]. According to the standard EN 459-1 [1], NHL is classified as NHL 2, NHL 3.5, and NHL 5; the corresponding compressive strength at 28 days in MPa is as follows: $2 \leq \text{NHL } 2 \leq 7$, $3.5 \leq \text{NHL } 3.5 \leq 10$, and $5 \leq \text{NHL } 5 \leq 15$.

The use of NHL mortars prevails presently for restoration works due to their good compatibility with the substrate material in terms of physical, chemical, and mechanical properties [5, 6]. That is to say, NHL mortars interact quite well with stones and blocks of masonry walls; the interventions with the materials are durable in time and do not originate spalling of the stones [7]. Moreover, NHL mortars are more appropriate than air-hardening or lime pozzolana ones when the early strength gain is essential [6]. Furthermore, NHL mortars are eco-efficient as they require low amount of energy during their production process and absorb CO_2 from the air while carbonating [6].

Knowledge on the mechanical properties of mortar is crucial to ensure a good performance of masonry structures [8]. In general, NHL mortars are well investigated in terms of compressive and flexural strengths [5, 9–11]. Recently, Garijo, Zhang, and Ruiz *et al.* [12, 13] have measured fracture energy, splitting tensile strength and characteristic length of such materials. At present time, the dynamic mechanical behavior of lime mortars is getting more attention due to the fact that most masonry structures are situated in zones of seismic activity, such as Lisbon (Portugal), L'Aquila (Italy), Lorca (Spain), Kathmandu (Nepal), Nairobi (Kenya), etc. Pereira and Lourenço [14] studied the dynamic compressive behavior of masonry specimens, clay brick, and mortar prisms by using a drop-weight tower. The corresponding strain rate range was from 2 to 200 s^{-1}. A commercial ready-mix mortar (Mapei Mape-Antique MC) was used for the fabrication of masonry and mortar specimens. The dynamic increase factor (DIF, a ratio of the dynamic response over the corresponding quasi-static one) 2.73 was obtained for the compressive fracture energy of the mortar specimens. Asprone *et al*. [15] analyzed the tensile behavior of a basalt fiber-reinforced natural hydraulic lime mortar at medium and high strain rates, using a hydropneumatic machine and a modified Hopkinson bar apparatus, respectively. The DIF for tensile strength was 5.11 at the strain rate 90 s^{-1}. For bending behavior, Chan and Bindiganavile [16] studied the strain rate sensitivity of plain and fiber-reinforced hydraulic lime mortar by adopting a universal testing machine and a drop-weight impact machine at strain rate range from 10^{-6} to 10 s^{-1}. Impact tests on notched beams with dimensions 100 mm × 100 mm × 350 mm were conducted; the notch depth was 12.5 mm and 2 mm in width, and the span was 300 mm. For plain hydraulic lime mortar, the results show that the DIF for modulus of rupture was 12 at the drop height 500 mm (corresponding to strain rate 10 s^{-1}), while it was 53 for fracture toughness. Moreover, the flexural behavior of hydraulic lime mortar is more sensitive to strain rate than fiber-reinforced hydraulic lime mortar. Later, the bond behavior between the stone masonry block and the plain and fiber-reinforced hydraulic lime mortar was also investigated by Bindiganavile *et al*. [17, 18]. The results show that there was an improvement in the bond strength due to polypropylene microfibers (20 mm in length)

but a difference in the fracture performance between the Portland cement-lime and hydraulic lime mortars. Whereas with the former, the fibers promoted failure through fracture in the stone block especially under dynamic loading conditions; with the latter, the fibers moved the failure plane from the interface to within the bulk mortar.

Nevertheless, there is still a need for the further understanding of the mechanical behavior of NHL mortars under quasi-static and dynamic loading conditions, especially for the latter. In this chapter, under quasi-static loading condition, an advanced mechanical characterization of NHL 3.5 mortars has been performed, such as elastic modulus, fracture energy, splitting tensile strength, and compressive and flexural strengths. Particularly, compressive strengths from prisms and cylinders were compared to study the size and shape influence. Moreover, the effects of dosage and production process on these properties were analyzed as well. Under dynamic loading condition, NHL mortar beams were tested at various loading rates (loading-point displacement rates) by using a servo-hydraulic testing machine, from the quasi-static one, 5.0×10^{-4} mm/s, to rate sensitive ones, 5.0×10^{-1} mm/s (intermediate loading rate) and 1.6×10^{1} mm/s (fast loading rate). The results show that the peak load and fracture energy are rate sensitive, which is mainly due to the viscous effect caused by the presence of free water in the porous structure.

2. Experimental procedure

2.1. Raw materials

The binder used for all seven types of mortars was a NHL 3.5, according to EN 459-1 [1]. It was supplied by "Socli, Italcementi group (France)" with an apparent particle density of 2.58 g/cm^3 and apparent density of 0.85 g/cm^3. Three types of aggregates were adopted in the fabrication process. The usual one was a commercial crushed limestone with maximum size of 4 mm; the rest were the crushed limestones with a maximum size of 2 mm and river sand with a maximum size of 4 mm. The particle-size distribution curves of the aggregates were determined in accordance with EN 1015-1 [19] and are shown in **Figure 1**. The apparent density and apparent particle density of each aggregate listed in **Table 1** were measured according to EN 1097-3 [20] and EN 1097-6 [21], respectively.

2.2. Mortar preparation

In total, seven types of mortars were prepared and tested (see **Table 2**). All of them presented a lime/aggregate volume ratio 1:3 as it is the one commonly used for the historical mortars [22, 23]. Volume proportions of compounds were converted to weight to obtain a convenient measurement for the mixing process. First of all, a benchmark mortar, named as NHL09C04M as a simplification, was fabricated with a water/lime volume ratio of 0.9, which provided a plastic consistency (between 140 and 200 mm), determined by the flow table test according to EN 1015-3 [24] and EN 1015-6 [25]. In addition, a crushed limestone aggregate with a maximum grain size of 4 mm and a metallic mold were used. The rest of the mortars were prepared by varying one aspect of the benchmark mortar, such as the water/lime ratio, the

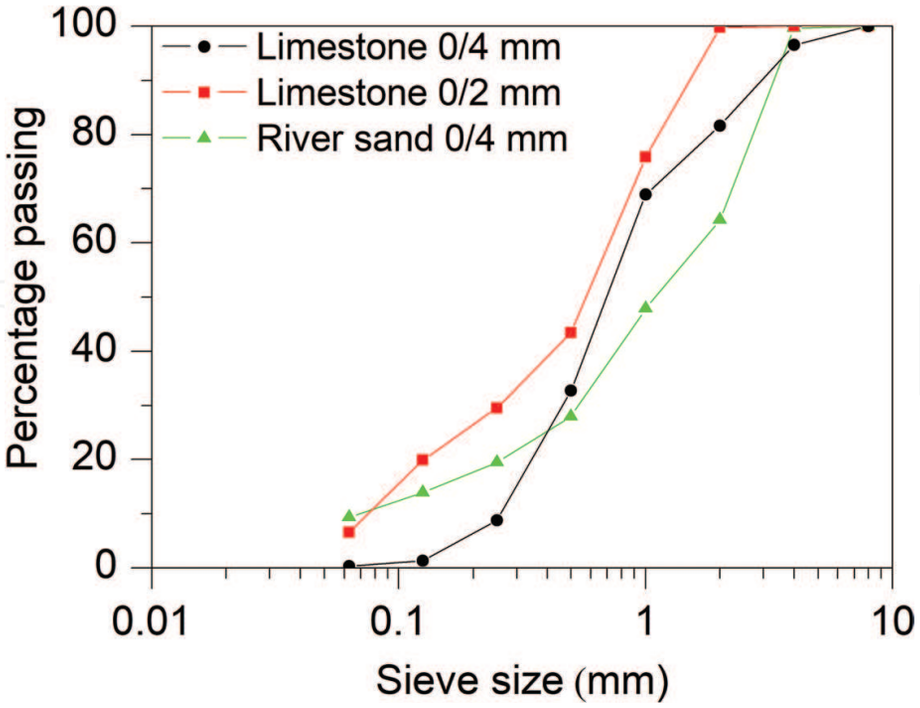

Figure 1. Aggregates grading curves.

Density	Standards	Crushed limestone 0/4 mm	Crushed limestone 0/2 mm	River sand 0/4 mm
Apparent density (g/cm^3)	EN 1097-3 [20]	1.82	1.81	1.46
Apparent particle density (g/cm^3)	EN 1097-6 [21]	2.68	2.74	2.59

Table 1. Apparent density and apparent particle density of the aggregates used.

maximum aggregate size, the aggregate type, the material of the mold, and the curing conditions (see **Table 2**). In order to isolate and quantify the influence of the type and maximum size of aggregate, materials of mold, and curing conditions on the mechanical properties of mortars, the water/lime ratio was kept constant as 0.9 instead of following the conventional procedure by adapting the water/lime ratio to obtain an approximately constant consistency as presented in the Refs. [5, 6, 9].

The mixing process was performed according to EN 1015-2 [26]. Both prismatic (40 × 40 × 160 mm) and cylindrical (75 mm in diameter and 150 mm in height) specimens were prepared. The mortar was poured in two layers when using the prismatic molds and in three layers instead when the cylindrical molds were used; each layer was compacted with 25 strokes of the tamper. All specimens were removed from the molds in 2 days after the fabrication according to EN 1015-11 [27].

2.3. Mechanical tests

The flexural, compressive, and splitting tensile strengths, elastic modulus, and fracture energy were measured by various types of tests as shown in **Figure 2**, at an age of 56 days. Moreover,

Mortar composition	Volumetric water/lime ratio	Consistency (mm)	Type of aggregate	Maximum grain size (mm)	Material of the mold	Curing conditions
NHL09C04M	0.9	150–155	Crushed limestone	4	Metallic	56 days in CC
NHL08C04M	0.8	130–135	Crushed limestone	4	Metallic	56 days in CC
NHL11C04M	1.1	238–240	Crushed limestone	4	Metallic	56 days in CC
NHL09C02M	0.9	120–125	Crushed limestone	2	Metallic	56 days in CC
NHL09R04M	0.9	180–187	River sand	4	Metallic	56 days in CC
NHL09C04W	0.9	150–155	Crushed limestone	4	Wooden	56 days in CC
NHL09C04MA	0.9	150–155	Crushed limestone	4	Metallic	7 days in CC and 49 in AC

CC, climatic chamber (RH: 97 ± 0.5%, 20 ± 0.5°C); AC, ambient laboratory conditions (RH: 50 ± 10%, 23 ± 3°C).

Table 2. Characteristics of the seven mortar compositions prepared.

the loading rate effect on fracture energy was studied by performing three-point bending tests on beams at various loading rates (loading-point displacement rates), 5.0×10^{-4} mm/s (quasi-static loading rate), 5.0×10^{-1} mm/s (intermediate loading rate), and 1.6×10^{1} mm/s (high loading rate), respectively.

2.3.1. Flexural and compressive strength

The flexural and compressive strengths were measured according to EN 1015-11 [27] by using the Instron 1011 testing machine. The flexural strength was obtained by a three-point bending test on three beams at a loading rate of 10 N/s and a span of 100 mm (see **Figure 2(a)**). It is worth noting that the anti-torsion supports were used for the test, which is specially important for quasi-brittle materials. That is to say, the beam rests on two rigid-steel cylinders placed on two supports which permit rotation out of the plane of the beam and rolling along the longitudinal axis of the beam with negligible friction.

The compressive tests were performed at a loading rate of 50 N/s on the six half prisms remaining from the bending tests, as presented in **Figure 2(b)**. The load was centered in the middle of the longest side by using a steel plate (40 mm × 40 mm × 10 mm). Moreover, an individualized ball-and-socket joint over the steel plate was used to reduce the eccentricity during the loading process.

2.3.2. Elastic modulus and compressive strength from cylinders

For studying the size and shape effects on the compressive strength, compressive tests were also performed on four cylinders (75 mm in diameter and 150 mm in height) at a loading rate of 10 N/s by using the Instron 8805 testing machine. Moreover, the elastic modulus was determined following the principles of EN 12390-13 [28] (see **Figure 2(c)**). Two clips (strain gauge

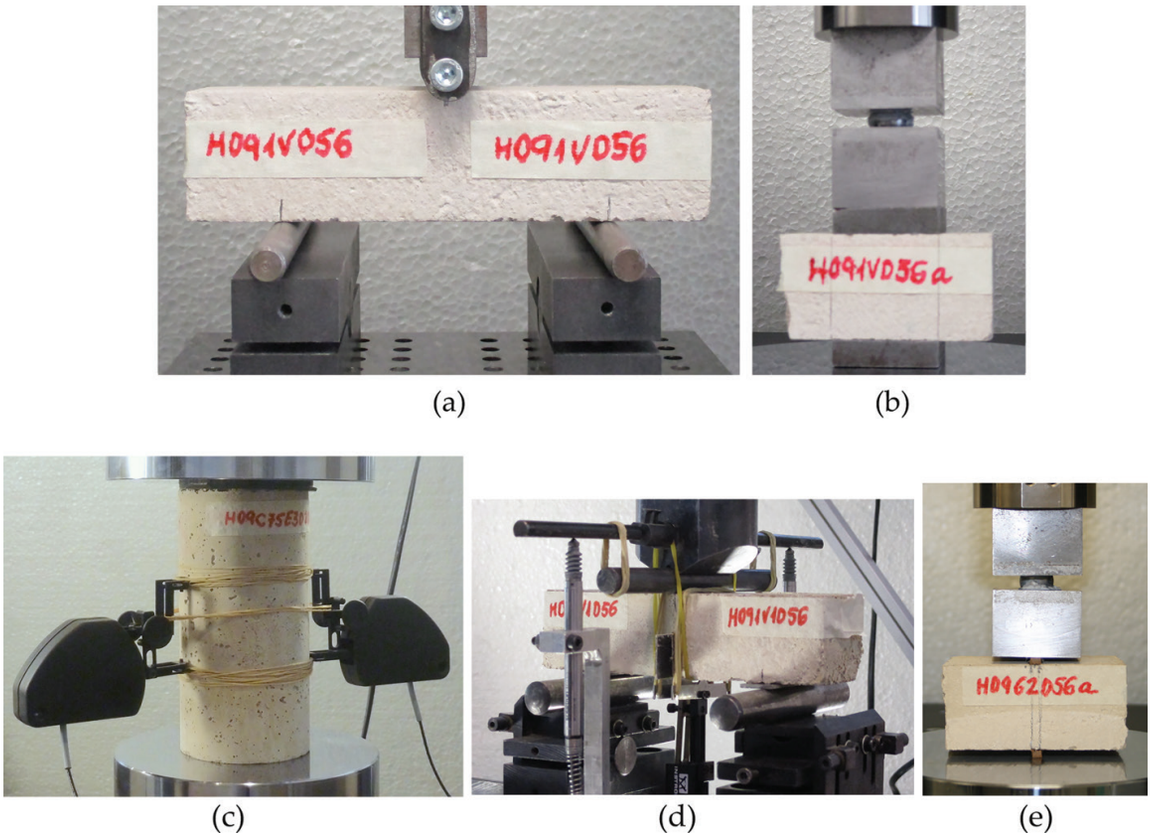

Figure 2. Tests for (a) flexural strength, (b) compressive strength, (c) elastic modulus and compressive strength from cylinders, (d) fracture energy and elastic modulus from prisms, and (e) splitting tensile strength.

extensometers Instron 2630) were used to measure the axial deformation. They were placed centrally in opposite generatrices of the specimen covering a span of 50 mm in order to avoid local constrictions caused by the friction of the specimen surface and the steel platens of the machine. Two rubber layers with 2 mm thickness each were used between the upper surface of the sample and the steel platen to keep away from contact problems due to the irregular roughness of the sample. In order to obtain a stable value, five repeat monotonic tests were conducted up to 30% of the compressive strength at a loading rate 10 N/s for each cylinder; the mean of the last three values measured was taken as the elastic modulus.

2.3.3. Fracture energy and loading rate effect

The fracture energy, defined as the energy required to open a unit area of crack surface, was measured through a three-point bending test by using the Instron 8805 testing machine, following the procedure recommended by the RILEM [29] and the improvements proposed by Planas, Guinea, and Elices [30–32] (see **Figure 2(d)**). The beams were the same size as those used for the flexural tests. A precast notch in the middle of the specimens was introduced by using a cardboard piece (2 mm in width and 20 mm in depth) during the fabrication. More detailed information on how to determine the fracture energy can be found in the Refs. [12, 13].

The tests were performed in the displacement control. In order to study the rate effect on the fracture energy, three various loading rates (loading-point displacement rates) were applied during the test from a quasi-static level (5.0×10^{-4} mm/s) to rate dependent (dynamic) levels (5.0×10^{-1} mm/s and 1.6×10^{1} mm/s). In such way, it took around 30 minutes and 0.3 seconds to finish the tests for the lowest and fastest loading rates, respectively. Three beams were tested at each loading rate. The corresponding strain rate, $\dot{\varepsilon}$, can be calculated approximately according to the Eq. (1):

$$\dot{\varepsilon} = \frac{6(D-a)\,\dot{\delta}}{S^2} \tag{1}$$

where $\dot{\delta}$ stands for the loading rate; D and S are the beam depth and span, respectively; and a is the notch depth.

2.3.4. Elastic modulus from prisms

When performing the three-point bending tests at quasi-static loading rate, an extensometer (strain gauge extensometer Instron 2620) was attached to the lower surface of the specimen to obtain the crack-mouth opening displacement (CMOD). In this way, the elastic modulus (E_{pr}) could be obtained from prisms by applying general Eqs. (2) and (3) for span/depth (S/D) ratios (β) between 2.5 and 16 [33]:

$$E_{pr} = 6\frac{Sa}{C_i B D^2}\upsilon_\beta(\alpha) \tag{2}$$

$$\upsilon_\beta(\alpha) = \upsilon_\beta(a/D) = 0.8 - 1.7\alpha + 2.4\,\alpha^2 + \frac{0.66}{(1-\alpha)^2} + \frac{4}{\beta}(-0.04 - 0.58\alpha + 1.47\,\alpha^2 - 2.04\,\alpha^3) \tag{3}$$

where C_i is the initial compliance determined from load-CMOD curve, $\upsilon_\beta(\alpha)$ is a dimensionless shape function depending on β, and the relative notch/depth ratio α. The other parameters of the beam have been previously defined.

2.3.5. Splitting tensile strength (indirect tensile strength)

The splitting tensile strength was measured through quasi-static splitting tensile tests (Brazilian tests) on four prismatic halves resulting from the preceding bending test for measuring fracture energy, following the procedure recommended by EN 12390-6 [34]. To conduct the test, the Instron 1011 testing machine was used, and the loading rate was set at 50 N/s. The proportion between the load-bearing width and the height of the specimens was maintained as low as 1/10 following the recommendations in [35–37]. The bearing strips were made of plywood, and they were placed in the middle of the longest side of the halves (see **Figure 2(e)**). The splitting tensile strength is determined as

$$f_t = 2F/\pi BD \tag{4}$$

where f_t is the splitting tensile strength, F is the maximum load, and B and D are the specimen width and depth, respectively, as mentioned previously.

2.3.6. Characteristic length

Once the splitting tensile strength (f_t), elastic modulus from cylinders (E_{cy}), and quasi-static fracture energy (G_F) are obtained, the characteristic length, l_{ch}, is calculated in accordance with Eq. (5). It is a parameter proposed by Hillerborg *et al*. [38] for fracture behavior, which is related to the length of the fracture process zone. It could be used to predict the brittleness of a material. As it decreases, brittle nature dominates and vice versa:

$$l_{ch} = E_{cy} G_F / f_t^2 \tag{5}$$

3. Results and discussion

In this section, the results of the experimental campaign described in Section 2 are presented. It is organized as follows: influence of dosage and production process on the mechanical properties of seven types of NHL mortars, size effect on the compressive strength, and the loading rate effect on the fracture behavior.

3.1. Influence of dosage and production process on the mechanical properties

In total, five influence factors on the mechanical properties of seven types of NHL mortars were studied, i.e., water/lime ratio, material of the mold, type and maximum size of the aggregates, and curing conditions. As explained in Section 2, a benchmark mortar was prepared, named as NHL09C04M (see **Table 2**). The influence of each factor was analyzed by varying an aspect of the mortar. That is to say, the influence of the water/lime ratio was studied among NHL08C04M, NHL09C04M, and NHL11C04M; the effect of the material of the mold was investigated by comparing NHL09C04W and the benchmark mortar, the influence of the type and maximum size of the aggregates through mortars NHL09R04M and NHL09C02M with the benchmark mortar, respectively. Finally, the impact of the curing conditions was obtained by comparing NHL09C04MA with the benchmark one. The detailed experimental results on the mechanical properties are listed in **Table 3**, f_{flex}, f_{cpr}, f_{ccy}, G_F, f_t, E_{cy}, E_{pr}, and l_{ch}, respectively, the flexural strength, compressive strength from prisms, compressive strength from cylinders, fracture energy at quasi-static loading rate, elastic modulus from cylinders, elastic modulus from prisms, and characteristic length. It is worth noting that for NHL09C04W, only the flexural and splitting tensile strengths (**Figure 3(a)** and **(c)**) were measured as the cylindrical wooden molds were not fabricated. Moreover, the notched beams were damaged when demolding the specimens from the prismatic wooden molds [12].

It is observed from **Table 3**, in general, the mechanical properties of NHL mortars are improved for low water/lime ratio when comparing the experimental results among NHL08C04M, NHL09C04M, and NHL11C04M, due to the fact that the open porosity increases with an

Mortar composition		f_{flex} (MPa)	f_{cpr} (MPa)	f_{ccy} (MPa)	G_F (N/m)	f_t (MPa)	E_{cy} (GPa)	E_{pr} (GPa)	l_{ch} (mm)
NHL09C04M	Mean	1.3	3.2	2.0	12	0.39	5.0	5.2	390
	Std. dev.	0.1	0.1	0.2	3	0.02	0.2	0.5	
NHL08C04M	Mean	1.3	4.2	2.7	13	0.51	5.4	6.0	260
	Std. dev.	0.1	0.3	0.3	1	0.01	0.6	0.2	
NHL11C04M	Mean	0.89	1.7	1.4	4.9	0.24	2.8	3.8	240
	Std. dev.	0.04	0.1	0.1	0.8	0.03	0.7	1.0	
NHL09C04W	Mean	1.7	3.5	—	—	0.57	—	—	—
	Std. dev.	0.1	0.1			0.05			
NHL09C02M	Mean	1.1	3.2	2.0	12	0.49	4.6	5.1	220
	Std. dev.	0.1	0.2	0.1	1	0.05	0.2	0.6	
NHL09R04M	Mean	0.96	2.3	1.5	10	0.38	4.2	4.4	280
	Std. dev.	0.06	0.1	0.1	2	0.03	0.2	0.4	
NHL09C04MA	Mean	0.91	2.4	1.5	8	0.34	2.8	3.2	190
	Std. dev.	0.02	0.1	0.1	1	0.03	0.4	0.6	

Table 3. Mechanical properties of NHL mortars at an age of 56 days.

increase in water/lime ratio which results in a weakening of the mortar structure and its mechanical properties [12]. Moreover, using wooden molds also benefits the mechanical properties as they absorb the excess of free water. The influence of the aggregate size is coupled with the effect of the water/lime ratio. According to the Ref. [6], larger coarse aggregates improve the resistance in a comparison among mortars with similar consistencies. However, this is achieved by adding more water to mortars with smaller aggregates, as they have a higher water demand, which modifies the water/lime ratio. In our case, NHL09C04M and NHL09C02M have the same water/lime ratio as 0.9. As both have similar mechanical properties, it could be due to the positive effect of a lower water/lime ratio offsetting the possible lower capacity of smaller aggregates.

NHL09C04M and NHL09R04M mortars were fabricated with crushed limestone and river sand, respectively. In a fresh state, NHL09R04M has a higher consistency (180–187 mm) than NHL09C04M (150–155 mm) for the same water/lime ratio. It is obvious that the crushed limestone aggregates exhibit better interlocking behavior than the river sands with round particles [39]. It should be noted if less water were added to NHL09R04M to get similar consistency as NHL09C04M, the mortar would be stronger.

The effect of the curing conditions were studied between NHL09C04MA, cured in the climatic chamber (RH: 97 ± 0.5%, 20 ± 0.5°C) for the first 7 days and at ambient laboratory conditions (RH: 50 ± 10%, 23 ± 3°C) for the rest 49 days, and NHL09C04M, cured in the climatic chamber for 56 days. The former presents lower mechanical properties than the latter. For example,

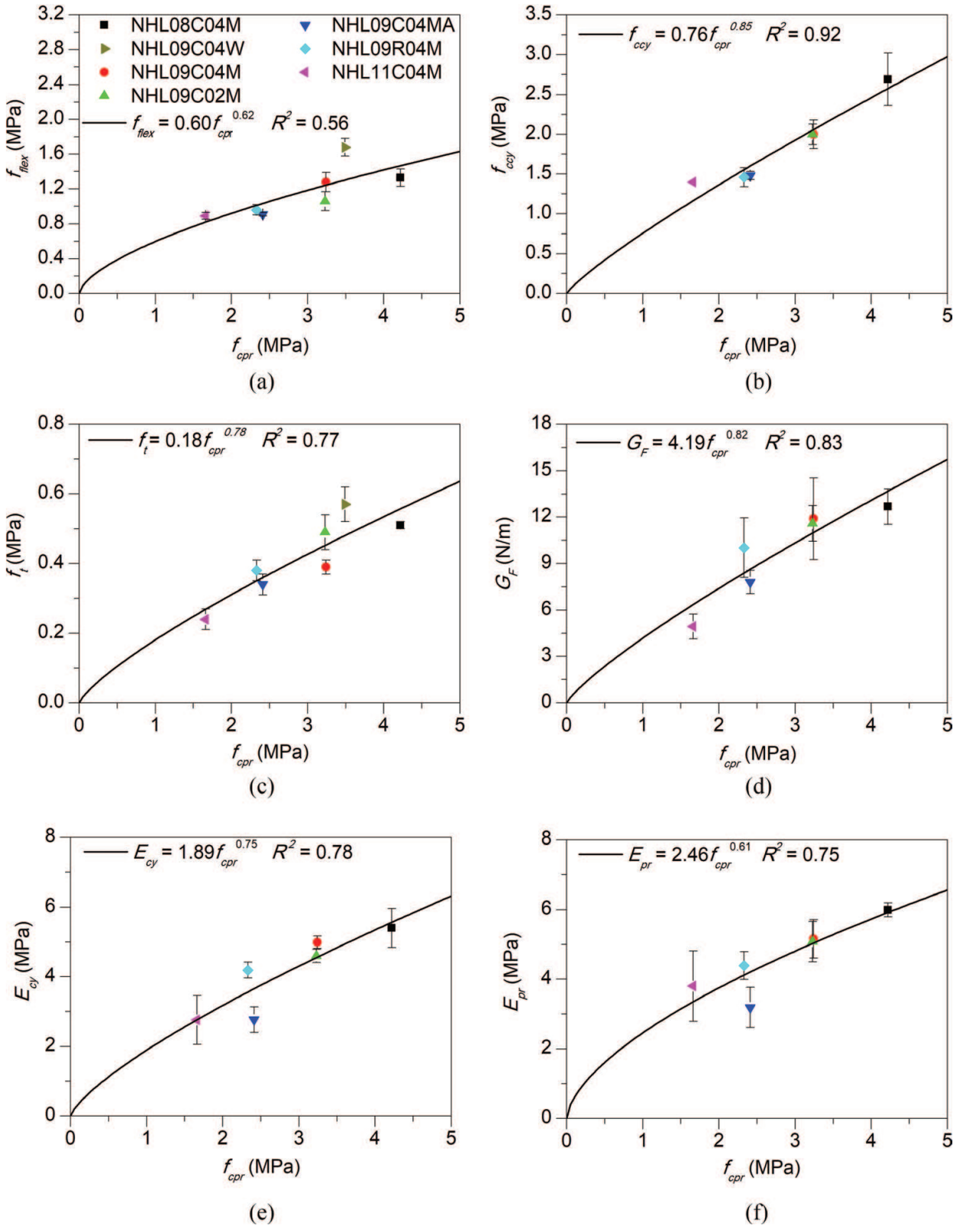

Figure 3. Relationship between compressive strength from prisms and other mechanical properties: (a) flexural strength, (b) compressive strength from cylinders, (c) splitting tensile strength, (d) fracture energy, (e) elastic modulus from cylinders, (f) elastic modulus from prisms.

their flexural strengths are 0.91 and 1.3 MPa, respectively. This is mainly due to the fact that high humid conditions favor the hydration of NHL mortars [9, 10, 12].

As mentioned in Section 2.3.6, characteristic length is an indicator of brittleness of quasi-brittle materials. The shorter a material is, the more brittle it is. It is clear that using river sand in the fabrication and curing at ambient laboratory make the mortars more brittle. Moreover, smaller aggregate size of the mortar favors the brittle behavior.

In **Figure 3**, various empirical equations relating some mechanical properties with the compressive strength from prisms were obtained (Eq. (6); **Table 4**) by fitting the experimental results. This could be useful for numerical simulations and structural design when only the compressive strength is measured owing to the convenience of performing the test. It is similar with the application of equations provided by the FIB Model Code [40] and ACI Building Code [41] for concrete. In most cases, R^2, the determination coefficient, is over 75%. However, for the flexural strength, it is only 56%, due to the fact that the result of the specimens fabricated in the wooden mold does not follow the trend. The equation used to do the empirical correlations is:

$$Y = m f_{cpr}^{n} \tag{6}$$

3.2. Size effect on compressive strength

From **Table 3** and **Figure 3(b)**, it is observed that there is a big difference between the compressive strength obtained from prisms and cylinders. For example, they are 4.2 and 2.7 MPa, respectively, for NHL08C04M, while 1.7 and 1.4 MPa for NHL11C04M, respectively. This could be due to improper curing throughout the specimen in the case of the cylinders, which are more massive than prisms [42]. However, this would not be the main cause as both specimens present similar densities and open porosities [12]. Instead, the difference is mainly because of geometry and size effects, which are confirmed by the following numerical simulation on the compressive tests of prisms.

The numerical model was created by using a commercial software, ATENA [43]. This program uses the finite element method and has nonlinear constitutive material models implemented,

Y	m	n
f_{flex}	0.60	0.62
f_{ccy}	0.76	0.85
f_t	0.18	0.78
G_F	4.19	0.82
E_{cy}	1.89	0.75
E_{pr}	2.46	0.61

Table 4. Values of adjusting parameters according to Eq. (6).

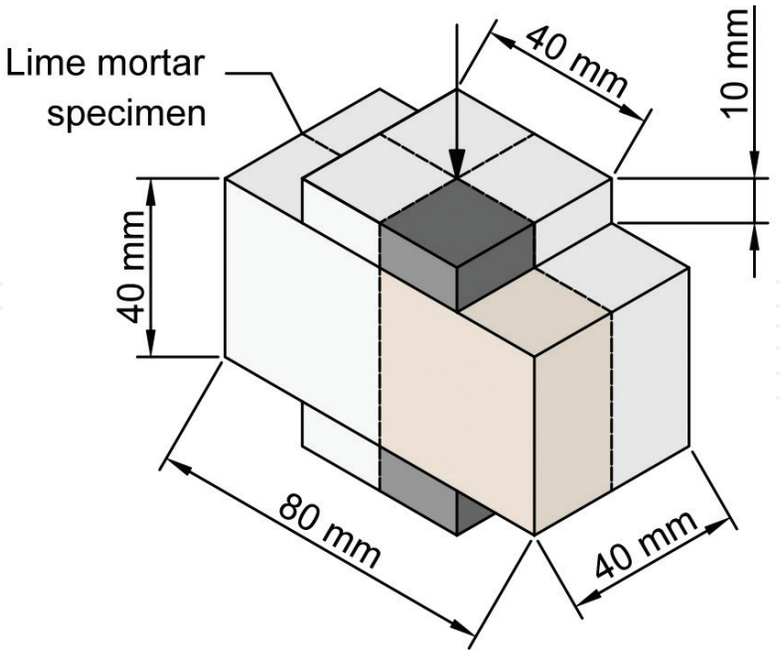

Figure 4. Geometry of the numerical model.

especially aimed for cohesive materials [13, 44]. The geometry of the model is formed by the mortar specimen itself and two metallic plates as used in the experimental test (see **Figure 4**). In order to reduce the number of finite elements and computing cost, symmetry was used in the model, defined by two vertical axes of symmetry. The material properties (E_{cy}, G_F, f_t, and f_c) were taken from the experimental results of mortars NHL08C04M (dry consistency) and NHL11C04M (fluid consistency), respectively (**Table 3**). Under the hypothesis that the compressive strength of cylinder is closer to the intrinsic compressive strength of the material, we adopted their corresponding values as f_c, instead of the corresponding to prisms. The metallic plates were defined as perfect linear elastic as their only function was to transmit the load and their strength was much higher than the one of the mortar [13].

In order to complete the comprehension of the possible size effect, two additional models of both mortars were performed by doubling the size of the original one once (80 mm × 80 mm × 160 mm) and twice (160 mm × 160 mm × 320 mm), respectively, and it followed the procedure described by del Viso *et al*. in [45]. Then, it was possible to obtain the nominal strength of each model, σ_N, as the ratio of the corresponding maximum loads and their respective bearing surfaces.

In **Figure 5**, the square of the nominal strength of the three models for each mortar, σ_N^2, is plotted against the inverse of Hillerborg's brittleness number, $1/\beta_H$ or l_{ch}/D. By adjusting a linear fitting of these three points, it is possible to obtain the asymptotic value of the compressive strength when the specimen depth, D, tends to infinite, that is to say, the intrinsic compressive strength of the material, σ_{inf} [13, 45]. This fitted line is defined in Eq. (7):

$$\sigma_N^2 = \sigma_{inf}^2 + \sigma_{inf}^2 A \frac{1}{\beta_H} \tag{7}$$

http://dx.doi.org/10.5772/intechopen.80852

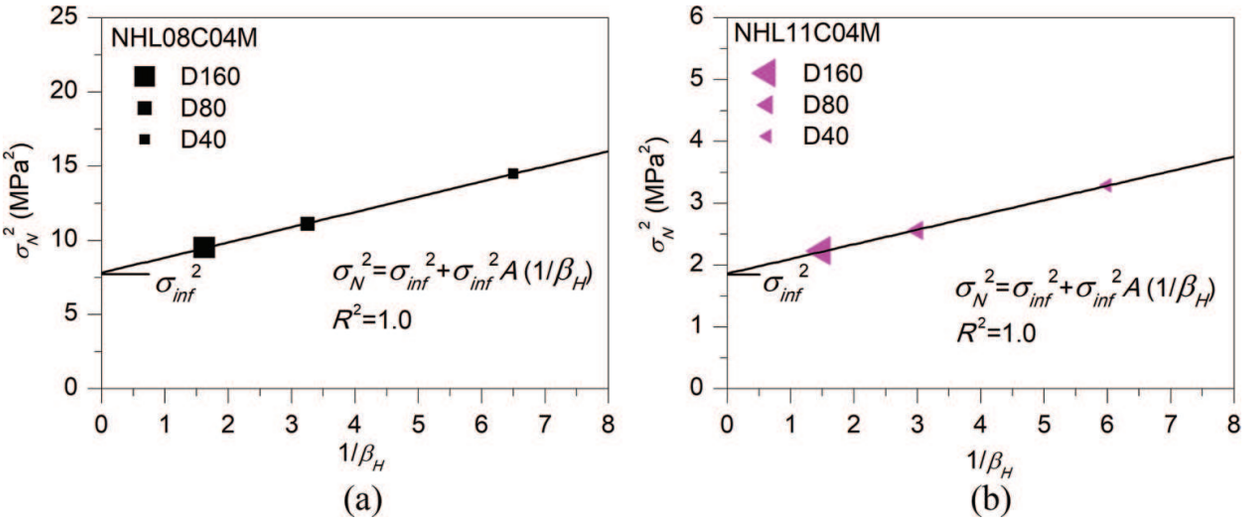

Figure 5. Regression for setting σ_{inf} and A for (a) NHL08C04M and (b) NHL11C04M.

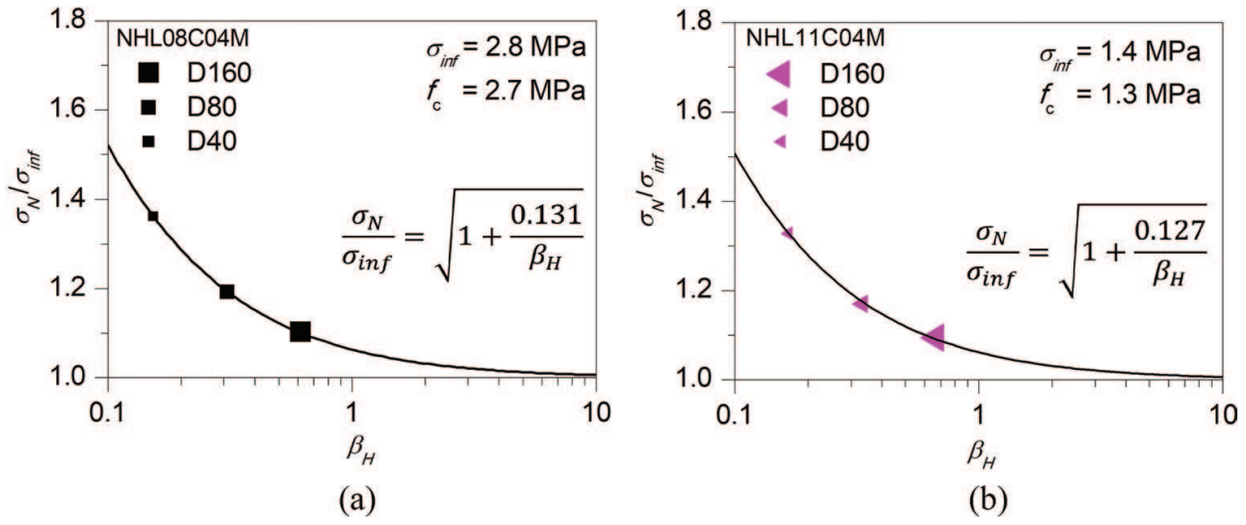

Figure 6. Size effect law for (a) NHL08C04M and (b) NHL11C04M.

where A is obtained from the slope of the fitted line of **Figure 5** for each mortar. With σ_{inf}, it is possible to obtain the non-dimensional values of σ_N (the ratio σ_N/σ_{inf}) and plot them related to β_H with a logarithmic scale (**Figure 6**). Then, it is possible to adjust one curve per mortar mix fitting these points. These two curves represent their size effect laws. As shown by them, for large specimen sizes, the size effect tends to disappear. In both cases, σ_{inf} is close to the compressive strength of cylinders, meaning that this value can roughly be considered as the intrinsic compressive strength of the material, instead of the compressive strength of the prisms.

3.3. Loading rate effect on the fracture behavior

In order to study the rate effect on the fracture behavior of NHL mortars, the benchmark mortar, NHL09C04M, was tested in three-point bending under three different loading rates,

Type of NHL specimens	Loading rate, $\dot{\delta}$ (mm/s)	Strain rate, $\dot{\varepsilon}$ (s^{-1})	Maximum load, P_{max} (N)	DIF for P_{max}	Fracture energy, G_F (N/m)	DIF for G_F	Water content (%)
Normal	5.0×10^{-4}	6×10^{-6}	99 (10)	1.0	12.2 (1)	1.0	2.52 (0.24)
	5.0×10^{-1}	6×10^{-3}	120 (10)	1.2	17.3 (1)	1.4	
	1.6×10^{1}	2×10^{-1}	140 (15)	1.4	22.8 (10)	1.9	
Dry	5.0×10^{-4}	6×10^{-6}	110 (20)	1.0	17.9 (2)	1.0	
	1.6×10^{1}	2×10^{-1}	110 (10)	1.0	22.5 (7)	1.3	

Table 5. Experimental results at various loading rates for NHL09C04M.

5.0×10^{-4} mm/s (quasi-static loading rate), 5.0×10^{-1} mm/s, and 1.6×10^{1} mm/s. **Table 5** presents the experimental results, where the values in brackets refer to the corresponding standard deviation. Moreover, an estimation of the strain rate, $\dot{\varepsilon}$, is included as well for comparison with results of the literature under other loading methods. The DIF is defined by the ratios of peak load (P_{max}) and fracture energy (G_F) to their corresponding quasi-static values. **Figure 7** shows the peak load and fracture energy obtained under three different loading rates.

From **Table 5** and **Figure 7**, it is observed that the maximum load and fracture energy of the NHL mortar increase with the loading rate. For example, their DIFs at the highest rate are 1.4 and 1.9, respectively.

The tendency of the rate effect on the peak load and fracture energy is also presented in **Figure 8**. Moreover, following Eqs. (8) and (9), curve fittings of the DIFs are derived from the experimental results in regard to the peak load and the fracture energy, respectively, by using the least squares method. These adjustments provide a correlation coefficient higher than 95%. Though the format of such equations is original for plain and steel fiber-reinforced concretes [46–49], they are still valid for NHL mortars:

$$DIF_{P_{max}} = 1 + 0.19 \left(\frac{\dot{\delta}}{\dot{\delta}_0} \right)^{0.29} \tag{8}$$

$$DIF_{G_F} = 1 + 0.44 \left(\frac{\dot{\delta}}{\dot{\delta}_0} \right)^{0.25} \tag{9}$$

where $\dot{\delta}_0$ is set as 1 mm/s. Such equations may be useful to predict the rate effect on the peak load and the fracture energy and when performing numerical simulations involving fracture on NHL mortars.

For understanding the cause of the loading rate dependency, six specimens (three per loading rate) were dried for 48 hours at 105°C and tested at the lowest and highest loading rates. The experimental results of the dry specimens are also presented in **Table 5**. Moreover, the comparison of the maximum DIF between the normal and dry lime mortars is shown in **Figure 9**. It is obvious that the rate effect of NHL mortar is mainly related with the movement of free water in pores. For example, for the dry NHL mortar, the peak load is almost

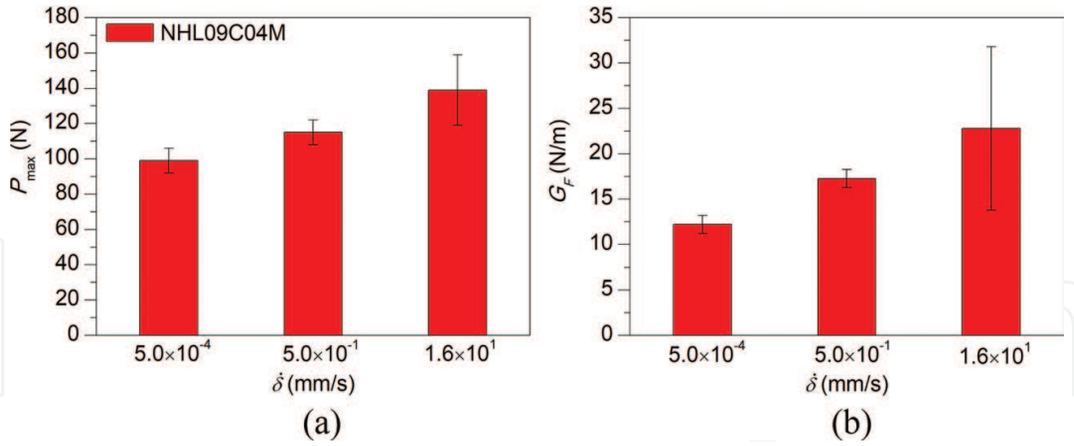

Figure 7. Peak load and fracture energy at various loading rates. (a) Peak load. (b) Fracture energy.

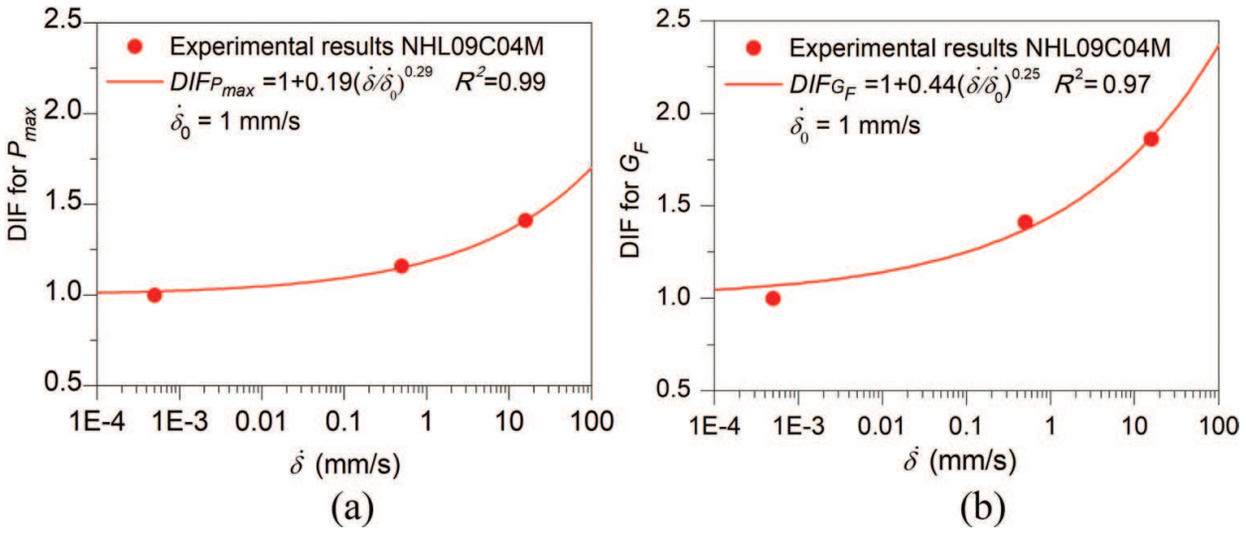

Figure 8. Loading rate effect on (a) peak load and (b) fracture energy.

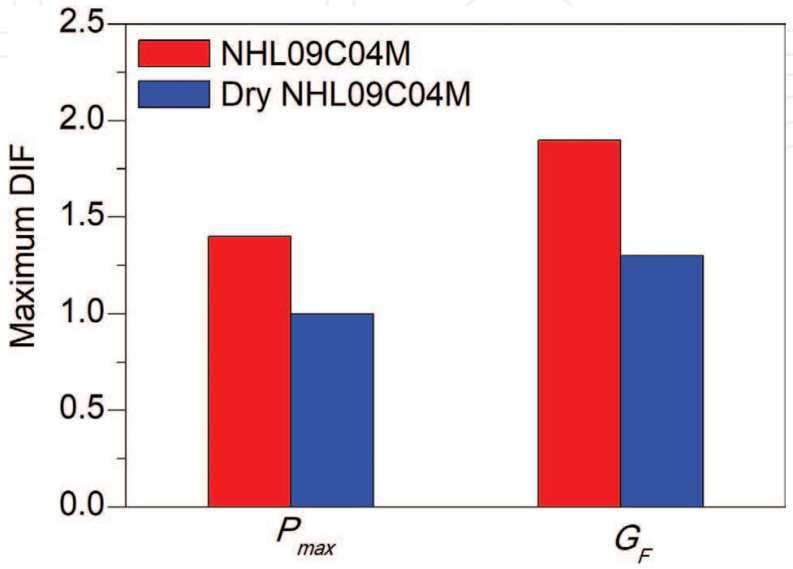

Figure 9. Maximum DIF of the normal and dry specimens of NHL09C04M.

constant at different loading rates, a 30% increase in fracture energy. However, for the normal NHL mortar, the DIFs of the peak load and fracture energy are 1.4 and 1.9, respectively.

4. Conclusions

In the chapter, the influence of five factors affecting the dosage and fabrication process of seven types of NHL 3.5 mortars on their mechanical properties was studied. Moreover, the shape and size effect on the compressive strength was disclosed by numerical simulation and experiments. Furthermore, the loading rate effect on the fracture energy was investigated as well.

Regarding the five influence factors on the mechanical properties, the results show that high water/lime ratios produce structural weakening and reduce mechanical properties. High relative humidity (97 ± 0.5%) is more suitable than ambient laboratory conditions for the hydration of the compounds of NHL mortars and for the increase of its ductility. Moreover, using wooden molds also improves these properties as they absorb the excess of free water. When maintaining constant water/lime ratios, using aggregates with higher grain size increases the mechanical properties. Mortars with river sand have lower mechanical properties. Certainly, if the water/lime ratio also varies at the same time, the tendency would be different.

There exists a big variation on the compressive strengths from prisms and cylinders; the ratio could reach 1.6. A numerical simulation analysis of the compressive test on prisms of two NHL mortars confirms that such variation is mainly due to the geometry and size effects.

With respect to the loading rate effect, from 5.0×10^{-4} to 1.6×10^{1} mm/s, on the fracture behavior of NHL mortar, it is obvious that the material is rate sensitive. The DIFs of the peak load and fracture energy are 1.6 and 1.9, respectively. Such phenomenon is mainly because of the viscous effects caused by the presence of free water in the porous structure.

Acknowledgements

The authors acknowledge the funding from the INCRECYT, the *Ministerio de Economía y Competitividad*, Spain, under grant BIA2015-68678-C2-1-R and from the *Junta de Comunidades de Castilla-La Mancha* (JCCM), *Fondo Europeo de Desarrollo Regional*, Spain, PEII-2014-016-P. L. Garijo thanks the funding from the scholarship FPU014/05186 given by the *Ministerio de Educación*, *Cultura y Deporte*, Spain, and J. J. Ortega from the scholarship 2017/759 awarded by JCCM, Spain. We also express our gratitude to Prof. Pere Roca, from *Universidad Politécnica de Cataluña*, Spain, for his advice on the dosage of the lime mortars.

Conflict of interest

None.

Author details

Lucía Garijo, XiaoXin Zhang, Gonzalo Ruiz*, José J. Ortega and Rena C. Yu

*Address all correspondence to: Gonzalo.Ruiz@uclm.es

School of Civil Engineering, University of Castilla-La Mancha, Ciudad Real, Spain

References

[1] BS EN 459-1. Building Lime—Part 1: Definitions, Specifications and Conformity Criteria. Brussels, Belgium: BSI; 2015. p. 52

[2] Silva BA, Pinto APF, Gomes A. Influence of natural hydraulic lime content on the properties of aerial lime-based mortars. Construction and Building Materials. 2014;**72**:208-218

[3] Arizzi A, Martinez-Huerga G, Sebastian-Pardo E, Cultrone G. Mineralogical, textural and physical-mechanical study of hydraulic lime mortars cured under different moisture conditions. Materiales de Construcción. 2015;**65**(318):1-11

[4] Lanas J, Arandigoyen M, Alvarez JI, Pérez Bernal JL, Bello MA. Mechanical behavior of masonry repair mortars: Aerial and hydraulic lime-based mixtures. In: 10th International Congress on Deterioration and Conservation of Stones Stockholm. 2004

[5] Lanas J, Bernal JLP, Bello MA, Galindo JIA. Mechanical properties of natural hydraulic lime-based mortars. Cement and Concrete Research. 2004;**34**(12):2191-2201

[6] Kalagri A, Karatasios I, Kilikoglou V. The effect of aggregate size and type of binder on microstructure and mechanical properties of NHL mortars. Construction and Building Materials. 2014;**53**:467-474

[7] Chan R, Bindiganavile V. Toughness of fibre reinforced hydraulic lime mortar. Part-1: Quasi-static response. Materials and Structures. 2010;**43**(10):1435-1444

[8] Haach VG, Vasconcelos G, Lourenço PB. Influence of aggregates grading and water/cement ratio in workability and hardened properties of mortars. Construction and Building Materials. 2011;**25**(6):2980-2987

[9] Lanas J, Sirera R, Alvarez JI. Study of the mechanical behavior of masonry repair lime-based mortars cured and exposed under different conditions. Cement and Concrete Research. 2006;**36**(5):961-970

[10] Grilo J, Silva AS, Faria P, Gameiro A, Veiga R, Velosa A. Mechanical and mineralogical properties of natural hydraulic lime-metakaolin mortars in different curing conditions. Construction and Building Materials. 2014;**51**:287-294

[11] Papayianni I, Stefanidou M. Strength-porosity relationships in lime-pozzolan mortars. Construction and Building Materials. 2006;**20**(9):700-705

[12] Garijo L, Zhang XX, Ruiz G, Ortega JJ, Wu ZM. The effects of dosage and production process on the mechanical and physical properties of natural hydraulic lime mortars. Construction and Building Materials. 2018;**169**:325-334

[13] Garijo L, Zhang XX, Ruiz G, Ortega JJ, Yu RC. Advanced mechanical characterization of NHL mortars and cohesive simulation of their failure behavior. Construction and Building Materials. 2017;**153**:569-577

[14] Pereira JM, Lourenço PB. Experimental characterization of masonry and masonry components at high strain rates. Journal of Materials of Civil Engineering. 2017;**29**(2):1-10

[15] Asprone D, Cadoni E, Iucolano F, Prota A. Analysis of the strain-rate behavior of a basalt fiber reinforced natural hydraulic mortar. Cement and Concrete Composites. 2014;**53**:52-58

[16] Chan R, Bindiganavile V. Toughness of fibre reinforced hydraulic lime mortar. Part-2: Dynamic response. Materials and Structures. 2010;**43**(10):1445-1455

[17] Islam MT, Chan R, Bindiganavile V. Stress rate sensitivity of stone masonry units bound with fibre reinforced hydraulic lime mortar. Materials and Structures. 2012;**45**(5):765-776

[18] Islam MT, Bindiganavile V. Dynamic fracture toughness of sandstone masonry beams bound with fiber-reinforced mortars. Journal of Materials in Civil Engineering. 2014; **26**(1):125-133

[19] BS EN 1015-1. Methods of Test for Mortar for Masonry—Part 1: Determination of Particle Size Distribution (By Sieve Analysis). BSI. 1998/A1; 2006. p. 8

[20] BS EN 1097-3. Test for Mechanical and Physical Properties of Aggregates Part 3: Determination of Loose Bulk Density and Voids. BSI; 1998. p. 10

[21] BS EN 1097-6. Test for Mechanical and Physical Properties of Aggregates Part 6: Determination of Particle Density and Water Absorption. BSI; 2013. p. 54

[22] Moropoulou A, Cakmak AS, Biscontin G, Bakolas A, Zendri E. Advanced byzantine cement based composites resisting earthquake stresses: The crushed brick/lime mortars of Justinian's Hagia Sophia. Construction and Building Materials. 2002;**16**(8):543-552

[23] Marastoni D, Benedetti A, Pela L, Pignagnoli G. Torque Penetrometric test for the in-situ characterisation of historical mortars: Fracture mechanics interpretation and experimental validation. Construction and Building Materials. 2017;**157**:509-520

[24] BS EN 1015-3. Methods of Test for Mortar for Masonry—Part 3: Determination of Consistence of Fresh Mortar (By Flow Table). BSI. 1999/A2; 2006. p. 10

[25] BS EN 1015-6. Merthods of Test for Mortar for Masonry—Part 6: Determination of Bulk Density of Fresh Mortar. BSI. 1998/A1; 2006. p. 8

[26] BS EN 1015-2. Methods of Test for Mortar for Masonry—Part 2: Bulk Sampling of Mortars and Preparation of Test Mortars. BSI. 1998/A1; 2006. p. 8

[27] BS EN 1015-11. Methods of Test for Mortar for Masonry—Part 11: Determination of Flexural and Compressive Strength of Hardened Mortar. BSI. 1999/A1; 2006. p. 12

[28] BS EN 12390-13. Testing Hardened Concrete Part 13: Determination of Secant Modulus of Elasticity in Compression. BSI; 2012. p. 10

[29] RILEM TC 50-FMC. Determination of the fracture energy of mortar and concrete by means of the three-point bend tests on notched beams. Materials and Structures. 1985; **18**:285-290

[30] Elices M, Guinea GV, Planas J. Measurement of the fracture energy using three point bend tests. 3. Influence of cutting the P-δ tail. Materials and Structures. 1992;**25**:327-334

[31] Elices M, Guinea GV, Planas J. Measurement of the fracture energy using three point bend tests. 1. Influence of experimental procedures. Materials and Structures. 1992;**25**:121-218

[32] Planas J, Elices M, Guinea GV. Measurement of the fracture energy using three point bend tests. 2. Influence of bulk energy dissipation. Materials and Structures. 1992;**25**:305-312

[33] Guinea GV, Pastor JY, Planas J, Elices M. Stress intensity factor, compliance and CMOD for a general three-point-bend beam. International Journal of Fracture. 1998;**89**(2):103-116

[34] BS EN 12390-6. Testing Hardened Concrete—Part 6: Tensile Splitting Strength of Test Specimens. BSI; 2009. p. 14

[35] Rocco C, Guinea GV, Planas J, Elices M. Size effect and boundary conditions in the Brazilian test: Theoretical analysis. Materials and Structures. 1999;**32**(220):437-444

[36] Iglesias I, Acosta B, Yu RC, Ruiz G, Aineto M, Acosta A. Study of mechanical characterization of ceramic specimens from a Brazilian test adaptation. Materiales de Construcción. 2011;**61**(303):417-429

[37] Rocco C, Guinea GV, Planas J, Elices M. Size effect and boundary conditions in the Brazilian test: Experimental verification. Materials and Structures. 1999;**32**(217):210-217

[38] Hillerborg A, Modéer M, Peterson PE. Analysis of crack formation and crack growth in concrete by means of fracture mechanics and finite elements. Cement and Concrete Research. 1976;**6**:773-782

[39] Lanas J, Alvarez JI. Masonry repair lime-based mortars: Factors affecting the mechanical behavior. Cement and Concrete Research. 2003;**33**(11):1867-1876

[40] FIB. Model Code 2010, Final Draft. Vol. 2012. Lausanne, Switzerland: FIB-Fédération Internationale du Béton. p. 311

[41] ACI 318-14. Building Code Requirements for Structural Concrete and Commentary. Farmington Hills: American Concrete Institute; 2014. p. 520

[42] Drougkas A, Roca P, Molins C. Compressive strength and elasticity of pure lime mortar masonry. Materials and Structures. 2016;**49**(3):983-999

[43] Cervenka V, Jendele L, Cervenka J. Computer Program of Nonlinear Finite Element Analysis of Reinforced Concrete Structures. Prague: Cervenka Consulting; 2009. pp. 1-142

[44] Poveda E, Ortega JJ, Ruiz G, Porras R, Carmona JR. Normal and tangential extraction of embedded anchor plates from precast facade concrete panels. Engineering Structures. 2016;**110**:21-35

[45] del Viso JR, Carmona JR, Ruiz G. Shape and size effects on the compressive strength of high-strength concrete. Cement and Concrete Research. 2008;**38**(3):386-395

[46] Zhang XX, Abd Elazim AM, Ruiz G, Yu RC. Fracture behavior of steel fibre-reinforced concrete at a wide range of loading rates. International Journal of Impact Engineering. 2014;**71**:89-96

[47] Zhang XX, Ruiz G, Tarifa M, Cendón D, Gálvez F, Alhazmi WH. Dynamic fracture behavior of Steel Fiber Reinforced Self-Compacting Concretes (SFRSCCs). Materials. 2017;**10**(11):1-16

[48] Zhang XX, Ruiz G, Yu RC, Poveda E, Porras R. Rate effect on the mechanical properties of eight types of high-strength concrete and comparison with FIB MC2010. Construction and Building Materials. 2012;**30**:301-308

[49] Zhang XX, Ruiz G, Yu RC, Tarifa M. Fracture behaviour of high-strength concrete at a wide range of loading rates. International Journal of Impact Engineering. 2009;**36**(10-11): 1204-1209